Dalton Transactions

ROYAL SOCIETY OF CHEMISTRY

PAPER

View Article Online
View Journal | View Issue

Check for updates

Cite this: *Dalton Trans.*, 2022, **51**, 18400

Symmetric CEST-active lanthanide complexes for redox monitoring†

Damien Mouchel dit Leguerrier,[a] Richard Barré,[a] Quentin Ruet,[b,c] Véronique Frachet,[b,c] Daniel Imbert,[d] Fabrice Thomas *[a] and Jennifer K. Molloy *[a]

Received 26th August 2022,
Accepted 25th October 2022

DOI: 10.1039/d2dt02776c

rsc.li/dalton

Two symmetric ligands harbouring two TEMPO radicals and two functionalized acetamide arms (R = OMe (**L_1**), CF_3 (**L_2**)) were prepared and chelated to lanthanide ions (Eu^{III}, Yb^{III} for both **L_1** and **L_2**, Dy^{III} for **L_1**). Luminescence measurements on the europium complexes support the coordination of a single water molecule. The TEMPO arms are magnetically interacting in **L_1** (and its complexes) but not in **L_2**. The TEMPO moieties can be reversibly oxidized into an oxoammonium (0.33–0.36 V *vs.* Fc^+/Fc) or reduced into a hydroxylamine (ill-defined redox wave, reduction by ascorbate), which are both diamagnetic. The europium complexes **$[Eu(L_1)]^{3+}$** and **$[Eu(L_2)]^{3+}$** in their hydroxylamine form exhibit a temperature dependent CEST effect, which is maximal at 25 °C (30%) and 37 °C (12%), respectively. The CEST activity is dramatically reduced in the corresponding nitroxide forms due to the paramagnetism of the ligand. The europium complexes show no cytotoxicity against M21 cell lines over long incubation times (72 h) at high concentration (40 μM).

1. Introduction

Redox switches have recently been proposed as a new alternative in smart responsive imaging in order to track and monitor the implication of reactive oxygen species (ROS) in several illnesses.[1] Increasing concentrations of ROS have been, for instance, reported in incurable (or hard to cure) diseases such as cancers or neurodegenerative disorders.[2–4] The detection of these molecular species is thus essential for a more complete understanding, diagnosis and treatment.[5]

Lanthanide complexes have been extensively used in medical imaging due to their fascinating optical and magnetic properties, lending them to ratiometric detection.[6] Responsive medical imaging has been increasingly reported with detection of metal ions, pH, redox conditions *etc.*[1,7,8] However, the development of lanthanide complexes, both luminescent and magnetic, which are sensitive to redox stimuli are not very well reported.[1] In particular, lanthanides ions are stable to redox stimuli, existing predominantly in their +III oxidation state (with some exceptions such as Eu^{II}/Eu^{III}).[1,9] Redox sensitive lanthanide complexes depend on a novel approach that combines a redox active ligand with the lanthanide ion.[10–12,37] The redox active ligand is thus the detector and the lanthanide ion then functions as a reporter with luminescent and magnetic responses. The Chemical Exchange Saturation Transfer (CEST) technique is a relatively new derivative technique of MRI, which utilises exchangeable protons on the ligand structure.[13,14] Selective irradiation followed by proton exchange results in a decrease in the bulk water signal. This technique presents a distinct advantage over classical MRI: selective irradiation can be employed in order to tailor the response.[15] The selective irradiation means that the activity can be switched on and off on demand.

CEST imaging has been shown to demonstrate changes in redox activity in biological systems such as the NAD^+/NADH couple. This activity is based on small changes in diamagnetic CEST.[16] Much larger shifts of the exchange proton signals can be achieved using paraCEST, limiting the risk of off-resonance.[17] We have recently reported redox active Eu^{III} complexes with amide pendant arms presenting a 12% CEST effect at 50 ppm upon reduction, demonstrating a proof of concept for redox sensitive paraCEST probes.[18,19] The CEST active complex showed a modest 6% switch in CEST activity between oxidised and reduced states. The asymmetric nature of these complexes was potentially the reason for the very low CEST effect observed. The CEST effect can indeed be dependent on the symmetry, which can increase the water exchange

[a]*Univ. Grenoble Alpes, CNRS, DCM, 38000 Grenoble, France. E-mail: jennifer.molloy@univ-grenoble-alpes.fr*
[b]*Institute for Advanced Biosciences, INSERM U1209, UMR CNRS 5309, Grenoble Alpes University, 38700 La Tronche, France*
[c]*EPHE, PSL Research University, 75014 Paris, France*
[d]*Univ. Grenoble Alpes, CEA, CNRS, IRIG-LCBM, 38000 Grenoble, France*

†Electronic supplementary information (ESI) available: CV curves, EPR, CEST and luminescence spectra. See DOI: https://doi.org/10.1039/d2dt02776c

rate. D. Sherry *et al.* suggested that symmetric complexes, particularly forming the SAP isomer could show increased CEST activity.[20] The design of symmetric systems containing both a CEST function and a redox active function was of immense interest to us, potentially increasing the number of equivalent protons and the CEST effect. The incorporation of two redox active arms instead of one could also increase the difference between the oxidized and reduced state. We herein report two symmetric macrocyclic ligands containing two CEST active amide functions and two redox active TEMPO functions. We demonstrate that the CEST effect is significantly improved in the europium complexes (up to 30%) in CH_3CN/H_2O in comparison to the previous series of compounds.

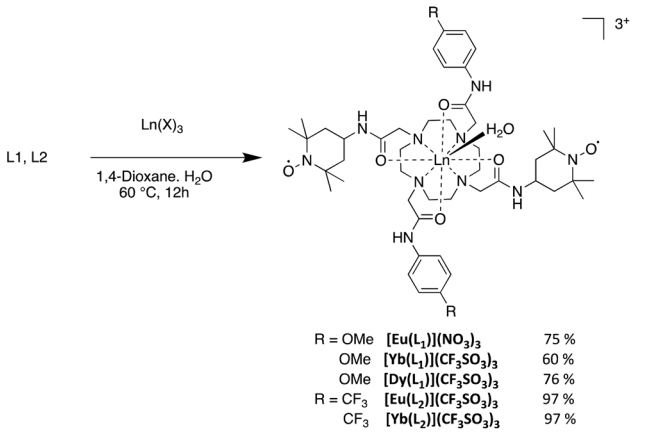

Scheme 2 Complexation of the ligands.

2. Results and discussion

2.1 Synthesis & characterisation

The synthesis of ligands $\mathbf{L_1}$ and $\mathbf{L_2}$ (Scheme 1) was performed *via* selective *N*-alkylation of the cyclen macrocycle. For this purpose we used the glyoxal cyclen precursor **1** (Scheme 1) and followed the procedure developed by Tripier *et al.*[21] This allowed specific functionalization with the 2-chloro-*N*-(4-methoxyphenyl)acetamide (**2OMe**)[22] or the 2-chloro-*N*-(4-trifluoromethylphenyl)acetamide ($\mathbf{2CF_3}$),[23] affording **3OMe** and $\mathbf{3CF_3}$, respectively, after treatment with PDA. The final ligands were generated *via* functionalization of the remaining two secondary amines with the TEMPO acetamide precursor **4**. This yields the symmetrically functionalised macrocycles $\mathbf{L_1}$ and $\mathbf{L_2}$, with a modest yield of 29% ($\mathbf{L_1}$) and 38% ($\mathbf{L_2}$) respectively (Scheme 1). The NMR characterization of the ligands was performed in the presence of ascorbate to reduce the nitroxide moieties into diamagnetic hydroxylamines. In particular, the resonances of the phenyl moieties are observed at δ = 6.84 and 7.53 ppm for $\mathbf{L_1}$ and 7.56 and 7.83 ppm for $\mathbf{L_2}$. The significant shielding in the case of $\mathbf{L_1}$ is a consequence of the strong electron donating ability of the methoxy substituent. Noteworthy, $\mathbf{L_2}$ exhibits a single peak at −63.6 ppm in ^{19}F NMR.

The Eu^{III}, Dy^{III}, Yb^{III} complexes were prepared by reaction in H_2O at pH 7.4, with the respective lanthanide salts (Scheme 2). The complexes were isolated by precipitation with yields of 60–97%. The complexes gave molecular signals corresponding to the tri-cations in ESI-MS, as exemplified by the peaks at m/z = 357.83, 359.63, 361.51 and 364.84, respectively for the Eu^{III}, Yb^{III}, Dy^{III} of the first series. The complexes $\mathbf{[Eu(L_2)]^{3+}}$ and $\mathbf{[Yb(L_2)]^{3+}}$ show two peaks in ^{19}F NMR, −61.5 and −77.6 for the first and −62.0, −78.7 for the second. Similar values have been reported for CF_3 containing Eu^{III} complexes.[24,25] The resonance at 78 ppm is assigned to the triflate counter-ion, the other to the trifluoromethyl substituent of the phenyl ring.

2.2 Electrochemistry

The ligands $\mathbf{L_1}$ and $\mathbf{L_2}$ are symmetric and possess two redox active functions. Hence, we conducted an electrochemical characterisation on both the ligands and the corresponding complexes. Electrochemical analysis was performed using cyclic voltammetry (CV) and rotating disk electrode (RDE) measurements in acetonitrile solution with 0.1 M tetra-*n*-butyl ammonium perchlorate (TBAP) as supporting electrolyte. Ferrocene was used as an external redox standard.

The ligands $\mathbf{L_1}$ and $\mathbf{L_2}$ each present an ill-defined irreversible reduction wave in the range −1 to −1.5 V *versus* Fc^+/Fc, which is assigned to the reduction of the nitroxide moieties. Upon scanning towards the anodic region, an irreversible oxidation wave was observed at 0.01 V and −0.04 V for $\mathbf{L_1}$ and $\mathbf{L_2}$, respectively. It is followed by a reversible oxidation wave at 0.33 V, which is assigned to the oxoammonium/nitroxide redox couple (Table 1). This latter potential is similar to that

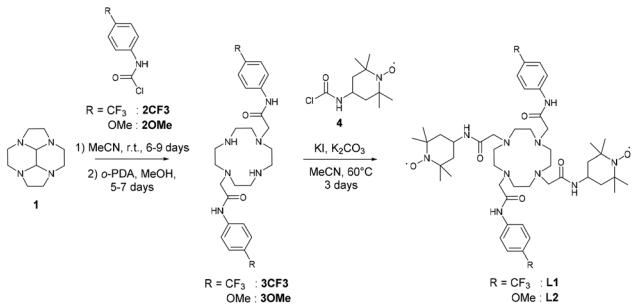

Scheme 1 Synthetic procedure for the formation of the ligands $\mathbf{L_1}$ and $\mathbf{L_2}$.

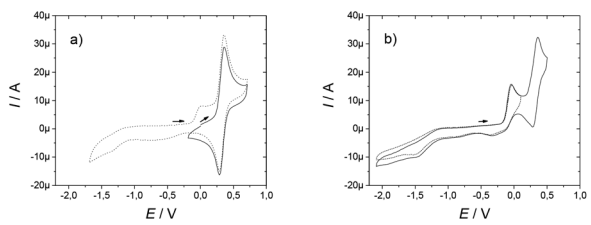

Fig. 1 CV curves of 0.5 mM CH_3CN solutions (+0.1 TBAP) of (a) $\mathbf{L_1}$ and (b) $\mathbf{L_2}$ at a carbon electrode. T = 298 K, scan rate = 0.1 V s^{-1}. All values reported with respect to the regular Fc^+/Fc redox couple that was used as an external reference.

Table 1 Electrochemical behaviour of the ligands and complexes[a]

Complexes	E_p [a]	$E_{1/2}$	Complexes	E_p [a]	$E_{1/2}$
$\mathbf{L_1}$	0.01	0.33	$\mathbf{L_2}$	−0.01	0.33
$[\mathbf{Eu(L_1)}]^{3+}$	0.04	0.36	$[\mathbf{Eu(L_2)}]^{3+}$	−0.05	0.33
$[\mathbf{Yb(L_1)}]^{3+}$	0.01	0.36	$[\mathbf{Yb(L_2)}]^{3+}$	0.03	0.33
$[\mathbf{Dy(L_1)}]^{3+}$	−0.01	0.36			

[a] From cyclic voltammetry experiments in CH_3CN (+0.1 M TBAP). The potentials are referenced to the regular Fc^+/Fc redox couple that was used as an external reference.

measured for the simple nitroxide arm **4** used as a reference, with an oxidation wave at 0.33 V. The irreversible oxidation wave seems to be associated with either an acido-basic equilibrium due to the nitroxide units[18] or the oxidation of the hydroxylamine into the nitroxide. Indeed, a proton-coupled electron transfer is expected to shift the oxidation wave close to the oxoammonium/nitroxide redox potential. The intensity of this peak increases when the scan is expanded to a larger range to include the nitroxide/hydroxylamine wave. RDE measurements showed that the reversible oxidation wave corresponded to two electrons, thus suggesting that the nitroxide moieties are electrochemically equivalent for each ligand (Fig. 1).

The complexes demonstrated electrochemical behaviour very similar to that of the ligands (Table 1). For example, the Eu^{III} complexes demonstrate an oxidation wave at 0.36 V and 0.33 V for $[\mathbf{Eu(L_1)}]^{3+}$ and $[\mathbf{Eu(L_2)}]^{3+}$ respectively, which can be assigned to the nitroxide oxoammonium couple, in addition to an irreversible system similar to the free ligand at 0.01 V and 0.05 V, respectively (Fig. 2).

No redox event was clearly observed that could be assigned to the Eu^{III}/Eu^{II} redox couple. Additionally, the metal ion has little or no effect on the oxidation potentials as each complex shows very similar $E_{1/2}$ values.

2.3 Luminescence spectroscopy

Luminescence spectroscopy can provide structural information from the f–f transitions for the Eu^{III} complexes and can be used to calculate the number of coordinated water molecules.[26] Luminescence spectra were recorded both in MeOH and CH_3CN/H_2O, due to solubility, *via* excitation in the ligand at 280 nm for $[\mathbf{Eu(L_1)}]^{3+}$ and $[\mathbf{Eu(L_2)}]^{3+}$. This yielded the distinctive transitions $^5D_0 \rightarrow {}^7F_{0-4}$ for the Eu^{III} luminescence corresponding to the main emissive levels of the species (Fig. 3). Excitation spectra confirmed sensitisation occurs *via* population of the ligand excited state. In particular, the $^5D_0 \rightarrow {}^7F_0$ is a quite intense and fine emission band suggesting low symmetry for the coordination sphere, with an intense emission for the $^5D_0 \rightarrow {}^7F_2$ commonly observed for DOTAM based derivatives.[38]

The emission profiles of $[\mathbf{Eu(L_1)}]^{3+}$ and $[\mathbf{Eu(L_2)}]^{3+}$ were very similar. As an example, the calculated ratios of the bands I ($^5D_0 \rightarrow {}^7F_2$)/I ($^5D_0 \rightarrow {}^7F_1$) were 3.1 and 3.6 respectively for the $[\mathbf{Eu(L_1)}]^{3+}$ and $[\mathbf{Eu(L_2)}]^{3+}$ in MeOH. The intensity ratios I ($^5D_0 \rightarrow {}^7F_4$)/I ($^5D_0 \rightarrow {}^7F_1$) gave 2.8 and 2.7 respectively, indicating closely related coordination spheres. The emission spectra recorded for the Yb^{III} complexes demonstrated only weak luminescence upon excitation at 280 nm for $[\mathbf{Yb(L_1)}]^{3+}$. Emission spectra for $[\mathbf{Yb(L_2)}]^{3+}$ showed no successful sensitisation of the excited state in this complex. This is potentially due to the high excitation wavelength permitting destabilisation of the excited state by non-radiative decay.

Luminescence lifetime measurements permitted the determination of the number of bound water molecules on the metal ion. Solutions of CH_3CN/H_2O and CD_3N/D_2O (10/90) were used to estimate the influence of OH oscillators on the luminescence decay. The luminescent lifetimes in deuterated and non-deuterated solvent were determined as τ = 0.48 ms and 1.43 ms respectively for H_2O and D_2O for the complex $[\mathbf{Eu(L_1)}]^{3+}$. These values were then extrapolated using the formulas of Horrocks and Parker, which take into consideration the NH oscillators in proximity to the coordination sphere of the Eu^{III} cation.[27,28] It must be stressed that the formula was initially developed for complexes in neat aqueous solutions. Assuming that the CH_3CN has very small influence on the parameters, we calculated one water molecule bound in the coordination sphere of the metal ion for both the $[\mathbf{Eu(L_1)}]^{3+}$ and $[\mathbf{Eu(L_2)}]^{3+}$ consistent with coordination complexes based on 9-coordinate DOTAM derivative structures. This was supported by performing the same measurements in MeOH using the Horrocks formula which also suggested one bound water molecule. Finally, the addition of ascorbate to reduce the nitroxide moieties results in an increase in the intensity of the emission bands by approximately one half. The quenching of the lanthanide luminescence in the oxidised form could be tentatively assigned to intramolecular quenching of the excited state due to the radical.

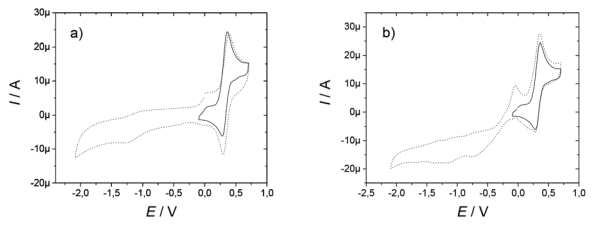

Fig. 2 CV curves of 0.5 mM CH_3CN solutions (+0.1 TBAP) of (a) $[\mathbf{L_1{\cdot}Eu}]^{3+}$ and (b) $[\mathbf{L_2{\cdot}Eu}]^{3+}$ at a carbon electrode. T = 298 K, scan rate = 0.1 V s^{-1}. All values reported with respect to the regular Fc^+/Fc redox couple that was used as an external reference.

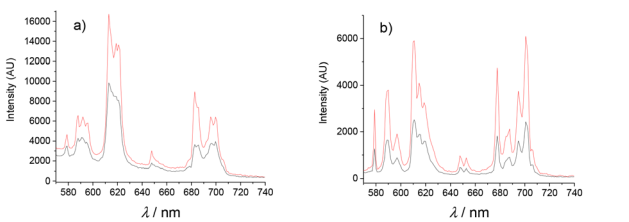

Fig. 3 Emission spectra of (a) $[\mathbf{Eu(L_1)}]^{3+}$ and (b) $[\mathbf{Eu(L_2)}]^{3+}$ in MeOH. Black: before addition of ascorbate; Red: after addition of one equivalent of ascorbate. T = 298 K.

2.4 Electron paramagnetic resonance

Electron Paramagnetic Resonance (EPR) measurements were utilised to gain insight into the environment of the nitroxide radicals and metal ion.

First, the spectra of the ligands in fluid CH_3CN solution mainly show an isotropic three-line pattern reminiscent of the TEMPO radical (Fig. 4). It is indeed centred at g_{iso} = 2.006 with the hyperfine splitting A_N of 1.6 mT. $\mathbf{L_1}$ demonstrates two additional features overlapped with the three line nitroxide pattern, which can be assigned to magnetic interactions between the nitroxide moieties.[29] These two features are in fact part of a five-line pattern overlapped with the dominant three-line pattern. The five-line splitting arises from exchange interactions between two nitroxide moieties, with the assumption that the coupling constant J is greater than the hyperfine splitting A_N. It is centred at the same g value and the resulting system exhibits hyperfine coupling constants that are half those of the isolated nitroxide. The spectrum of $\mathbf{L_2}$ does not feature such peculiarities, suggesting different positioning and thus interaction of the nitroxide arms.

Hence, the EPR spectrum of $\mathbf{L_1}$ supports the presence of a conformation that places the nitroxides units in a favourable situation for magnetic interactions between the two redox functions.

Both $\mathbf{[Eu(L_1)]^{3+}}$ and $\mathbf{[Eu(L_2)]^{3+}}$ exhibit isotropic spectra very similar to those of the corresponding ligands, with only the resonances of the nitroxide unit (see ESI†), unsurprising considering the weak magnetic moment of the Eu^{III} ion.

The ytterbium and dysprosium ions cannot be detected at room temperature due to their fast relaxation. In both cases the spectra were recorded at low temperature. Below 20 K an anisotropic nitroxide signature is observed around g = 2.00 for $\mathbf{[Yb(L_1)]^{3+}}$, with outermost broad resonances covering the 320–370 mT region (Fig. 5). The spectra recorded at different microwave powers show the same behaviour, confirming that it is not due to saturation effects. The most likely origin for these features is a magnetic coupling between the nitroxides units and the ytterbium ion. However, the nature of the ground spin state and the associated zero field splitting parameters could not be determined due to the significant linewidth. It is worth noting that no such resonances are observed for $\mathbf{[Yb(L_2)]^{3+}}$. Hence the phenyl para substituents play a role in orientating the nitroxide moieties, although the details remain yet unclear.

After reduction with sodium ascorbate, the complex $\mathbf{[Yb(L_1)]^{3+}}$ demonstrates well-defined resonances at g = 5.47, 4.35 and 3.60, with intensity ratios corresponding to the natural abundances of the Yb(III) isotopes. In comparison, the complex $\mathbf{[Yb(L_2)]^{3+}}$ shows a less defined resonance at g = 5.41. This behaviour is reminiscent of isolated Yb(III) complexes, confirming reduction of the TEMPO moiety.

The same behaviour is observed for the dysprosium complexes (see ESI†). More specifically, $\mathbf{[Dy(L_1)]^{3+}}$ displays the features of magnetically coupled system.

2.5 CEST activity

The addition of two substituted phenyl substituents (CF_3 and OMe) provides NH exchangeable protons which have been previously shown to demonstrate significant CEST activity.[22,30] The ligands $\mathbf{L_1}$ and $\mathbf{L_2}$ thus provide three potential CEST active moieties, the NH of the amide arms, the NH of the acetamide function and the coordinated water molecule. Selective irradiation of each of the exchangeable protons on the ligand at their Larmor frequency saturates their magnetisation. It is transferred by chemical exchange to bulk water, leading to a decrease in the water peak intensity. In order to observe a CEST effect the ligand proton exchange rate needs to be in the intermediate to slow exchange regime.[31]

The paraCEST spectra of $\mathbf{[Ln(L_1)]^{3+}}$ and $\mathbf{[Ln(L_2)]^{3+}}$ were recorded at 25 °C at pH 7.4 in a $H_2O : CH_3CN$ (2 : 1) mixture at 25 μT.

In its nitroxide form, the complex $\mathbf{[Eu(L_1)]^{3+}}$ presents a paramagnetically shifted resonance at 46 ppm from bulk water, exhibiting a CEST effect of 4% at 25 °C (Fig. 6). This peak can be assigned to the H_2O molecule coordinated to the lanthanide ion compared to reported literature resonances for coordinated H_2O.[20,32,33] From the ratio of intensities of the ligand proton resonance and the water peak the CEST effect was estimated to 4%. Reduction of the nitroxide unit to the hydroxylamine using ascorbate results in an increase of this peak at 46 ppm to 30%. This is much larger than that reported in our previous work with simple amide arms.[18]

This difference of 26% is significant and could potentially be interesting in the development of new CEST probes, however before such projections could be undertaken the solubility problems need to be resolved. Variable temperature measurements were performed to determine if the water

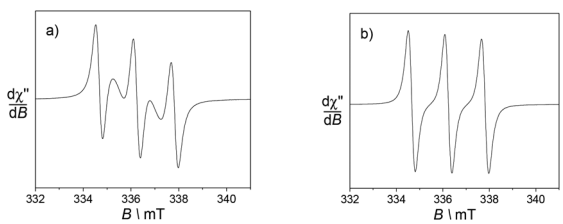

Fig. 4 X band EPR spectra of 0.5 mM CH_3CN solutions of the ligands (a) L_1 and (b) L_2. Microwave freq. 9.42 GHz; power, 3.5 mW; modulation amp., 0.2 mT; freq. 100 KHz. T = 293 K.

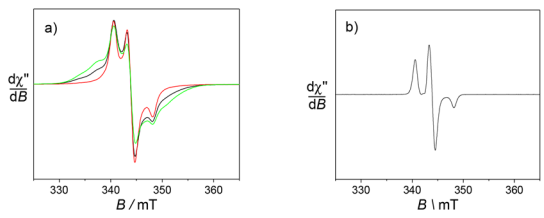

Fig. 5 X-band EPR spectra of 0.45 mM aqueous solutions (+10% glycerol) of (a) $\mathbf{[Yb(L_1)]^{3+}}$ and (b) $\mathbf{[Yb(L_2)]^{3+}}$. Microwave freq. 9.63 GHz, power 0.8 mW; mod. amp. 0.4 mT, freq. 100 KHz; (a) T = 4 (green), 10 (black), 20 (red) K; (b) T = 10 K.

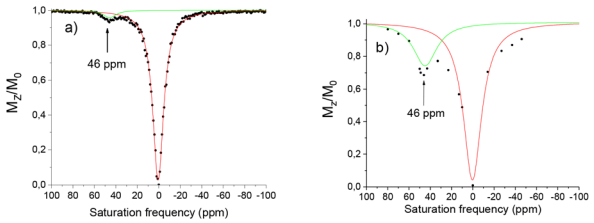

Fig. 6 Z spectra of a 20 mM H_2O : CD_3CN (2 : 1) solution of $[Eu(L_1)]^{3+}$ in a HEPES buffer (0.07 M, pH 7.4). (a) Nitroxide form, (b) hydroxylamine form generated by chemical reduction using 2 eq. of ascorbate. B_0 = 11.7 T, B_1 = 25 μT, irradiation time = 4 s, T = 298 K.

exchange rate is limiting. The maximum CEST activity was observed at 25 °C at 30%, decreasing to 21% at 37 °C (Fig. 7). The residence time of the water molecule was calculated *via* Omega plot[34] (variation of the CEST intensity as a function of the pulse irradiation strength) to be 380 μs, decreasing to 310 μs at 37 °C, suggesting that the water exchange rate is optimal.

In the case of $[Eu(L_2)]^{3+}$ in its nitroxide form only a weak shoulder is observed (under the same conditions as $[Eu(L_1)]^{3+}$). Complexes containing functional groups with CF_3 moieties have been reported to demonstrate significantly different water exchange rates due to fluorous and π-stacking interactions.[30] For example Allen *et al.*, demonstrate an 80 fold difference between the exchange rates in Gd^{III} phenyl CF_3 and OMe substituted complexes.[35] The CF_3 functionalised complex thus entered into a slow/intermediate exchange regime and presented no visible CEST activity at ambient temperature.

Variable temperature measurements demonstrate at 37 °C that a CEST peak becomes more defined at 40 ppm with an intensity of 12%, suggesting that the CEST activity, similar to the example above could be limited by the water exchange rate. Variable temperature measurements demonstrate an exchange rate of 2450 s^{-1} at 15° and 3270 s^{-1} at 37 °C. The absence of CEST signal at ambient temperature is most likely due to this slow exchange (Table 2).

The corresponding dysprosium complex $[Dy(L_1)]^{3+}$ demonstrated no CEST activity in both the oxidised and reduced forms, under the same conditions. The $[Yb(L_1)]^{3+}$ complex shows no CEST activity in the oxidised form. Reduction using sodium ascorbate results in a CEST spectrum presenting two

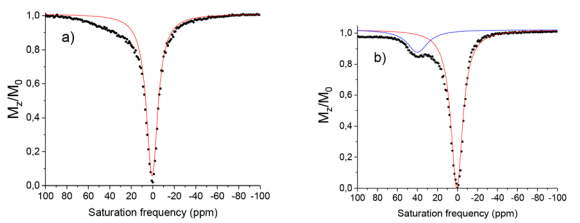

Fig. 7 Z spectra of a 20 mM H_2O : CD_3CN (2 : 1) solution of $[Eu(L_2)]^{3+}$ in a HEPES buffer (0.07 M, pH 7.4) under its hydroxylamine form generated by chemical reduction using 2 eq. of sodium ascorbate. (a) T = 298 K, (b) T = 310 K. B_0 = 11.7 T, B_1 = 19 μT, irradiation time = 4 s.

Table 2 CEST parameters for the reduced complexes[a]

Complex	T (°C)	δ (ppm)	CEST (%)	k_{ex} (s^{-1})	τ_M (μs)
$[Eu(L_1)]^{3+}$	15	50	10	2450	410
$[Eu(L_1)]^{3+}$	25	45	30	2650	380
$[Eu(L_1)]^{3+}$	37	37	21	3270	310
$[Eu(L_1)]^{3+}$	45	27	18	nd	nd
$[Eu(L_2)]^{3+}$	25	41	4	nd	nd
$[Eu(L_2)]^{3+}$	37	40	12	4000	250
$[Eu(L_2)]^{3+}$	45	34	8	nd	nd

[a] 20 mM solution of the complexes reduced by 2 eq. of sodium ascorbate. B_0 = 11.7 T; B_1 = 19 μT; T = 298 K; mixture H_2O : CD_3CN (2 : 1), [HEPES] = 0.07 M à pH 7.4; irradiation time = 4 s.

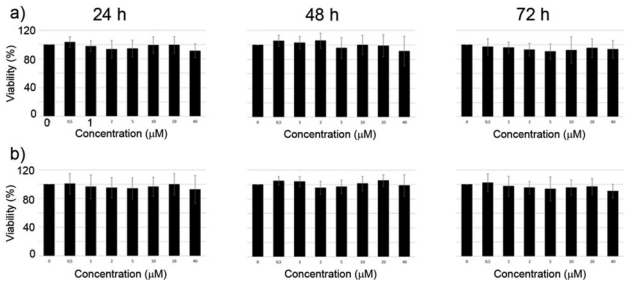

Fig. 8 Cellular viability of M21 cells after treatment with increasing amounts of: (a) $[Eu(L_1)]^{3+}$ and (b) $[Eu(L_2)]^{3+}$ (from MTT assays). The results were expressed as a percentage of the vehicle treated cells. Data shown are the mean ± SD of three independent experiments. The concentrations are 0, 0.5, 1, 2, 5, 10, 20, 40 μM from the first to the last column for each graph.

potential CEST resonances very close to the bulk water signal at −10 ppm and −20 ppm. These signals increase to 12% and 4% respectively upon reduction, however further studies were difficult due to their proximity to the H_2O bulk signal. Indeed, saturation could allow some offset resonance. These resonances are tentatively assigned to the acetamide exchangeable protons similar to those reported for similar complexes.[36] The oxidised and reduced $[Yb(L_2)]^{3+}$ complex shows no well-defined CEST peak, with only a weak shoulder for the reduced species. This complex was thus not studied further.

2.6 Cytotoxicity

The cytotoxicity of the complexes was investigated by MTT assays on M21 cell line. Due to the limited hydrosolubility of the complexes the medium contains 2% DMSO in H_2O. The cells were incubated with the complexes and the viability was determined after 24 h, 48 h and 72 h. Over the whole range of concentrations investigated (1–40 μM) the complexes did not demonstrate any cytotoxicity (Fig. 8).

3. Conclusions

In summary two series of lanthanide(III) complexes $[Ln(L_1)]^{3+}$ and $[Ln(L_2)]^{3+}$ were prepared from symmetrical DOTA ligands appended by two TEMPO and two substituted (OMe, CF_3)

phenylacetamide arms. Luminescence measurements demonstrated the presence of one water molecule in the first coordination sphere, with a similar coordination environment in both series of complexes. The TEMPO moiety could be reversibly oxidized into an oxoammonium function. It can be also reduced by a biological reductant like ascorbate into hydroxylamine. EPR measurements unravel interspin interactions in the ligand $\mathbf{L_1}$, which suggests a conformation distinct from $\mathbf{L_2}$. Such interaction is preserved in the complexes and at the solid state. It has been reported in some europium macrocycles that the CF_3 substituents of pendent phenyl groups are sufficiently fluorophilic to interact together, driving π–π interactions between the aromatics.[30] This results in a shielding of the coordinated water molecule from the bulk and subsequent lowering of the rate of exchange. Even if the shorter linker in our case certainly decreases the degree of freedom of the pendent phenylacetamide arms, this behaviour might nicely explain the absence of interspin interactions between the TEMPO units of $\mathbf{[Eu(L_1)]^{3+}}$, the two phenylacetamide arms hindering the coordination site.

Complex $\mathbf{[Eu(L_1)]^{3+}}$ is CEST active in both in its oxidised and reduced forms, with a peak at 46 ppm attributed to the coordinated water. The CEST effect is however much greater in the reduced form (30%) than in the oxidized form (4%) in mixed solvent conditions (that can exhalt slightly the reported values). This difference can be attributed to the acceleration of the relaxation rate due to the paramagnetism of the nitroxide. On the other hand, complex $\mathbf{[Eu(L_2)]^{3+}}$ demonstrates almost no CEST activity at 25 °C, but an increase of the temperature to 37 °C results in a 12% effect at 40 ppm of 12%. This indicates that the water exchange is limited in this case.

Altogether, these results suggest that these redox active lanthanide complexes could be interesting probes of redox state. Further studies are in progress to increase the CEST response and the solubility of these probes before they can be interesting for bimodal targeted imaging.

4. Experimental

4.1 Materials and methods

All chemicals were of reagent grade and were used without purification. NMR spectra were recorded on a Bruker AM 400 (^{1}H at 400 MHz) spectrometer. Chemical shifts are quoted relative to tetramethylsilane (TMS). Mass spectra were recorded on an ESI/QTOF Waters Xevo G2-S apparatus. The FTIR spectra were recorded using a Nicolet iS10 spectrometer on crystalline material (ATR mode). Luminescence data were recorded both at room and low temperature using an FLS-1000® (Edinburgh Instruments) equipped with automatic filters to remove the harmonic bands. Quartz cuvette with 1 cm optical path was used. For visible detection a PMT RP928 was used cooled at −20 C and for NIR, a InGAs was used cooled using pelletier. The signals were analysed with the Origin lab Origin Pro software. Lifetimes are averages of 3 independent determinations with a calculated Chi-square <2. Data and lifetimes were also confirmed on a Fluorolog FL3-22 spectrometer from Horiba-Jobin Yvon-Spex equipped with a double grating excitation monochromator and an iHR320 imaging spectrometer. X-band EPR spectra were recorded on a Bruker EMX Plus spectrometer equipped with a Bruker Helium flow cryostat and a dual mode cavity. Electrochemical measurements were carried out using a Biologic SP300 potentiostat. Experiments were performed in a standard three-electrode cell under argon atmosphere. A glassy carbon disc electrode (3 mm diameter), which was polished with 1 mm diamond paste, was used as the working electrode. The auxiliary electrode was a platinum wire, while the reference was an $Ag/AgNO_3$ 0.01 M in CH_3CN. All the potentials are given *vs.* the Fc^+/Fc redox couple, which was used as standard.

4.2 CEST protocols

Z spectra of the Eu^{III} complexes were recorded at 11.7 T (corresponding to a 500 MHz proton Larmor frequency) using a Bruker Avance III spectrometer equipped with a Prodigy cryo probe. The paramagnetic complexes were dissolved at a concentration of 20 mM in $H_2O:CD_3CN$ (66 : 33 v : v) solution. The complexes were analysed in their oxidised form. Spin lattice relaxation times were recorded in order to adjust the relaxation time D1 (<5 × T1) between 4 and 15 s. Z spectra were acquired with an irradiation time of 4 s at 19–25 μT and between 2.4 and 19 μT for saturation power study. The water signal is calibrated to 0 ppm and the spectral irradiation offset within a range of +100 ppm and −100 ppm for Eu^{III} complexes and +100 and −600 ppm for the Dy^{III} signals, between +250 ppm and −100 for Yb^{III} complexes relative to the water resonance. To obtain each spectrum an accumulation of 200 points was collected. The saturation transfer experiments were carried out between 15 and 45 °C by irradiating the Eu^{III} complexes samples at increments of 1 ppm in the frequency range ±100 ppm. The Yb complexes samples at increments of 1 ppm in the frequency range ±100 ppm, then at increments of 5–10 ppm in the frequency range +100 and +250 ppm. The Dy complexes samples at increments of 1 ppm in the frequency range ±100 ppm, then at increments of 5 ppm in the frequency range −100 and −600 ppm. Data were processed manually by integrating the area below the water signal. The percent saturation transfer (ST%) was calculated by the following formula: $ST = (1 - I/I_0)$ where I is the intensity of the water signal at a given irradiation frequency and I_0 is the maximum intensity of the water signal (off-resonance pre-saturation). After completion of all this sequence, 2 equivalents of sodium ascorbate were added in the solution. The complex is then in the "reduced form". The sequence is then reapplied following the same protocol.

4.3 Cell cultures

Human melanoma cell line M21 was purchased from ATCC (Manassas, VA, USA). Cells were cultured in DMEM medium supplemented with 10% (v/v) fetal calf serum (FCS) and 2 mM glutamine (Thermo Fisher Scientific, Courtaboeuf, France). Cells were maintained at 37 °C in a 5% CO_2-humidified atmosphere and tested to ensure freedom from mycoplasma con-

tamination. All cell lines were used within 5–50 passages of thawing the original stocks.

4.4 MTT assay

M21 cells were seeded into 96-well plates (1.5×10^3 cells per well) in 100 µl of culture medium. After 24 h, cells were treated with the lanthanide(III) complexes at various concentrations. Following incubation for 24 h, 48 h or 72 h, 10 µl of a MTT (3-(4,5-dimethylthiazol-2-yl)-2,5-diphenyltetrazolium bromide) stock solution (Euromedex, Mundolsheim, France) in PBS at 5 mg ml^{-1} was added in each well and the plates were incubated at 37 °C for 2 h. To solubilize water-insoluble purple formazan crystals, 100 µl of SDS 10%/HCl 0.1% solution was added. After 24 h, absorbance was measured on an ELISA reader (Tecan, Männedorf, Switzerland) at a test wavelength of 570 nm and a reference wavelength of 650 nm.

4.5 Synthetic procedures

2OMe and **2CF$_3$** were synthesised according to literature procedures.[22,23] **4** was synthesised according to literature procedure.[19]

3OMe (1,7-(*N*-(4-methoxyphenyl)acetamide)-1,4,7,10-tetraazacyclododecane). A solution of glyoxal protected cyclen **1** in 6 mL of MeCN (0.50 g, 2.6 mmol) was added slowly to a solution of **2OMe** (1.02 g, 5.2 mmol)[22] in MeCN (10 mL). KI (1.71 g, 10.3 mmol, 4 eq.) was then added to the mixture and stirred at room temperature for 6 days. The precipitate was removed by filtration and a white powder was obtained in quantitative yield (100%). This powder was dissolved in MeOH and *o*-phenylenediamine (*o*-PDA, 1.1 eq.) was added. The solution was stirred for 1 week under argon, the reaction was filtered and the solvents were removed *in vacuo*. The red oil was purified using DCVC chromatography (eluent from cyclohexane 100%, cyclohexane/dcm; 50/50; v/v, to MeOH 100%). After evaporation of solvents, it afforded compound **3OMe** (1.30 g, quantitative yield) as a pale yellow solid. ^{1}H NMR (400 MHz, MeOD) δ = 7.40 (d, J = 8.7 Hz, 4H), 6.67 (d, J = 8.7 Hz, 4H), 3.70 (s, 6H), 3.62 (s, 4H), 3.35–3.28 (cyclen). ^{13}C NMR (100 MHz, MeOD) δ = 170.7, 157.9, 132.3, 122.9, 114.9, 56.2, 55.9, 51.3, 44.4. FT-IR (solid, cm^{-1}): 3419, 3246, 3046, 2935, 2834, 2766, 1652, 1601, 1537, 1508, 1442, 1414, 1300, 1236, 1025, 830. HRMS (*m*/*z*): calcd for $C_{26}H_{38}O_4N_6$ $[M + H]^+$: 499.30273; found, 499.30200.

3CF$_3$ (1,7-(*N*-(4-trifluoromethyl)acetamide)-1,4,7,10-tetraazacyclododecane). **2CF$_3$** (1.71 g, 7.2 mmol) was added to a solution of glyoxal protected cyclen, **1** (0.70 g, 3.6 mmol) in MeCN (50 mL) containing KI (1.20 g, 7.2 mmol, 2 eq.). The mixture was then stirred at room temperature for 6 days. The precipitate was removed by filtration and a white powder was obtained in quantitative yield (100%). This powder was dissolved in MeOH and a solution of PDA (1.1 eq.) was stirred for 5 days under argon. Upon completion, the solvents were removed *in vacuo*. The red oil was dissolved in THF (40 mL) and stirred overnight. The precipitate was filtrated to afford compound **3CF$_3$** in 72% yield. ^{1}H NMR (400 MHz, MeOD) δ = 7.69 (d, J = 8.5 Hz, 4H), 7.30 (d, J = 8.7 Hz, 4H), 3.71 (s, 4H), 3.31–2.89 (m br, 16H). ^{13}C NMR (100 MHz, MeOD) δ = 171.8, 142.8, 126.9, 120.7, 68.9, 56.4, 51.4, 44.4, 26.5, 24.2. ^{19}F NMR (375 MHz, MeOD) δ = −63.8. FT-IR (solid, cm^{-1}): 3690, 3443, 3342, 3166, 3024, 2920, 2831, 2771, 1686, 1644, 1617, 1583, 1528, 1412, 1322, 1254, 1164, 1104, 1065, 1015, 938, 841. HRMS (*m*/*z*): calcd for $C_{26}H_{32}F_6N_6O_2$ $[M + H]^+$: 575.25637; found, 575.25446.

L$_1$ (1,7-(*N*-(4-methoxyphenyl)acetamide)-4,10-(*N*-(2′,2′,6′,6′-tetramethyl-1′-oxyl-4′-piperidyl)-amide-1,4,7,10-tetraazacyclododecane). The nitroxide derivative **4** (0.525 g, 2.1 mmol)[18] was added to a solution of **3OMe** (0.637 g, 1 mmol) in MeCN (50 mL) containing K_2CO_3 (0.552 g, 4 mmol, 4 eq.) and KI (0.664 g, 4 mmol, 4 eq.). The mixture was then stirred at 60 °C for 3 days. The solvents were removed *in vacuo* and the mixture was purified using DCVC chromatography (eluent gradient from dichloromethane 100%, CH_2Cl_2/MeOH; 50/50; v/v). After evaporation of solvents, it afforded **L$_1$** as an orange solid (0.267 g, 29%). Reduction with sodium ascorbate was used to characterize the ligand by NMR. ^{1}H NMR (400 MHz, $CDCl_3$): δ = 7.70 (s, 2H), 7.53 (s, 2H), 8.28), 6.82 (s, 2H), 6.77 (s, 2H), 3.73 (m, 8H), 3.65 (s, 4H), 3.24 (s, 4H), 3.07 (s, 4H), 2.87 (s, 4H), 2.81 (s, 4H), 1.30–1.0 (m, 32H TEMPOH). ^{13}C NMR (125 MHz, $CDCl_3$): δ = 206.5, 157.4, 70.1, 62.7, 58.0, 53.2, 31.4, 30.5, 29.2, 22.2, 18.1, 13.6, 13.4, 0.47. FT-IR (solid, cm^{-1}): 3406, 3229, 3085, 2974, 2927, 2861, 1615, 1574, 1504, 1462, 1363, 1323, 1239, 1177, 1084, 1025, 959, 833. HRMS (*m*/*z*): calcd for $C_{48}H_{77}O_8N_{10}$ $[M]^+$, 921.59204. Found, 921.59137. Elem. anal. calcd for $C_{48}H_{85}N_{10}O_{12}I$ (**L$_1$**, I^- + $4H_2O$): C, 51.4104; H, 7.6561; N, 12.4941. Found: C, 51.34; H, 7.59; N, 12.42.

L$_2$ (1,7-(*N*-(4-trifluoromethylphenyl)acetamide)-4,10-(*N*-(2′,2′,6′,6′-tetramethyl-1′-oxyl-4′-piperidyl)-amide-1,4,7,10-tetraazacyclododecane). The nitroxide derivative **4** (0.275 g, 1.1 mmol, 2 eq.) REF was added to a solution of **3CF$_3$** (0.306 g, 0.56 mmol) in MeCN (30 mL) containing K_2CO_3 (0.309 g, 2.2 mmol, 4 eq.) and KI (0.186 g, 1.1 mmol, 2 eq.). The mixture was then stirred at 70 °C for 13 days, filtered on celite and the solvents were removed *in vacuo*. The mixture was purified using DCVC chromatography (eluent from DCM 100% to DCM/MeOH; 50/50; v/v, to EtOH/NH_4OH; 50/50; v/v). After evaporation of solvents, it afforded compound **L$_2$** (0.211 g, 38%) as an orange solid. Reduction with sodium ascorbate was used to characterize the ligand. ^{1}H NMR (400 MHz, MeOD) δ = 7.83 (d, J = 8.6 Hz, 4H), 7.56 (d, J = 8.6 Hz, 4H), 4.14 (tt, J = 12.3 Hz, J = 3.7 Hz, 2H), 1.79 (d, J = 12.5 Hz, 4H), 1.44 (t, J = 12.2 Hz, 4H), 1.17 (d, J = 4.0 Hz, 24H). ^{13}C NMR (100 MHz, $CDCl_3$) δ = 179.3, 163.8, 126.9, 120.7, 74.3, 73.5, 64.9, 59.9, 55.6, 46.1, 45.7, 42.7, 32.8, 8.0. ^{19}F NMR (375 MHz, MeOD) δ = −63.6. FT-IR (solid, cm^{-1}): 3435, 3211, 3049, 2981, 2941, 2358, 1684, 1602, 1539, 1452, 1322, 1234, 1165, 1112, 1067, 848. HRMS (*m*/*z*): calcd for $C_{48}H_{71}O_6N_{10}F_6$ $[M]^+$: 997.54568; found, 997.54512.

4.6 General procedure for the synthesis of the complexes

To a solution of the ligand (0.06 mmol) in a mixture of 1,4-dioxane and water 1 : 1 (10 mL) was added 0.06 mmol of the metal (1 eq.) under its triflate salt (except for **[Eu(L$_1$)]$^{3+}$**, nitrate salt). The solution was stirred and heated at 50 °C for 1 day.

The solvents were evaporated under reduced pressure and the residue was solubilized in minimum of methanol, precipitated in ether and centrifuged.

$[Yb(L_1)]^{3+}$ $(CF_3SO_3)_3$. Orange powder in 60% yield. ^{1}H NMR (400 MHz, MeOD): δ = 108.9, 102.8, 99.8, 69.9, 21.1, 20.4, 17.8, 16.4, 15.4, 7.4, −24.8, −28.3, −30.0, −34.4, −57.3, −58.8. FT-IR (solid, cm^{-1}): 3444, 3255, 3094, 2980, 2942, 2873, 1622, 1572, 1513, 1463, 1276, 1239, 1163, 1082, 1027, 962, 833, 636. ESI-MS (*m*/*z*): calcd for $C_{48}H_{76}O_8N_{10}YbCF_3SO_3$ $[M]^{2+}$: 621.74; found, 621.73, 613.61; calcd for $C_{48}H_{76}O_8N_{10}Yb$ $[M]^{3+}$: 364.84; found, 364.95.

$[Eu(L_1)]^{3+}$ $(NO_3)_3$. Orange powder in 75% yield. ^{1}H NMR (400 MHz, MeOD): δ = 17.46, 7.76, 7.09, 6.75, 4.21, 3.91, 3.53, 3.48, 1.17, −1.89, −5.49, −7.26, −9.17. FT-IR (solid, cm^{-1}): 3402, 3251, 3080, 2976, 2936, 1620, 1569, 1511, 1462, 1301, 1240, 1178, 1082, 1029, 961, 834. ESI-MS (*m*/*z*): calcd for $C_{48}H_{76}O_8N_{10}EuNO_3$ $[M]^{2+}$: 567.75; found, 567.76; calcd for $C_{48}H_{76}O_8N_{10}Eu$ $[M]^{3+}$: 357.83; found, 357.85.

$[Dy(L_1)]^{3+}$ $(CF_3SO_3)_3$. Orange powder in 76% yield. ^{1}H NMR (400 MHz, MeOD): δ = 49.0, 15.6, 1.27, −81. FT-IR (solid, cm^{-1}): 3406, 3229, 3085, 2974, 2927, 2861, 1615, 1574, 1504, 1462, 1363, 1323, 1239, 1177, 1084, 1025, 959, 834. ESI-MS (*m*/*z*): calcd for $C_{48}H_{76}O_8N_{10}DyCl$ $[M]^{2+}$, 559.74; found, 559.74; calcd for $C_{48}H_{76}O_8N_{10}Dy$ $[M]^{3+}$, 361.51; found, 361.51.

$[Yb(L_2)]^{3+}$ $(CF_3SO_3)_3$. An orange powder in 97% yield. **^{19}F NMR** (375 MHz, D_2O) δ = −62.0, −78.7; **^{1}H NMR** (400 MHz, MeOD) δ = no signal; **IR**: 3296, 2982, 2949, 2341, 1682, 1549, 1460, 1396, 1278, 1238, 1223, 1157, 1028, 636.

$[Eu(L_2)]^{3+}$ $(CF_3SO_3)_3$. An orange oil in 97% yield. **^{19}F NMR** (375 MHz, MeOD) δ = −61.5, −77.6; **^{1}H NMR** (400 MHz, MeOD) δ = no signal; **IR**: 3450, 3296, 2989, 2926, 2355, 1682, 1557, 1460, 1393, 1276, 1240, 1224, 1158, 1028, 637.

Conflicts of interest

There are no conflicts to declare.

Acknowledgements

The authors thank the French National Research Agency in the framework of the "Investissements d'avenir" program (ANR-15-IDEX-02), Labex ARCANE and CBH-EUR-GS (ANR-17-EURE-0003) and the French National Agency for Research, program Co-Lantha (ANR-17-CE07-0034) for financial support. This work was performed under the auspices of the COST Action AC15209, EURELAX. The ICMG Platform (FR 2607) is acknowledged for the analytical support.

References

1 S. M. Pinto, V. Tomé, M. J. F. Calvete, M. M. C. A. Castro, É. Tóth and C. F. G. C. Geraldes, *Coord. Chem. Rev.*, 2019, **390**, 1–31.
2 K. L. Eales, K. E. R. Hollinshead and D. A. Tennant, *Oncogenesis*, 2016, **5**, e190.
3 M. W. Dewhirst and S. R. Birer, *Cancer Res.*, 2016, **76**, 769.
4 J. P. B. Connor, J. K. R. Boult, Y. Jamin, M. Babur, K. G. Finegan, K. J. Williams, R. A. Little, A. Jackson, G. J. M. Parker, A. R. Reynolds, J. C. Waterton and S. P. Robinson, *Cancer Res.*, 2016, **76**, 787.
5 J.-T. Hou, M. Zhang, Y. Liu, X. Ma, R. Duan, X. Cao, F. Yuan, Y.-X. Liao, S. Wang and W. Xiu Ren, *Coord. Chem. Rev.*, 2020, **421**, 213457.
6 S. Lacerda and É. Tóth, *ChemMedChem*, 2017, **12**, 883–894.
7 Q. Meng, M. Wu, Z. Shang, Z. Zhang and R. Zhang, *Coord. Chem. Rev.*, 2022, **457**, 214398.
8 A. C. Harnden, D. Parker and N. J. Rogers, *Coord. Chem. Rev.*, 2019, **383**, 30–42.
9 D. Mouchel Dit Leguerrier, R. Barré, J. K. Molloy and F. Thomas, *Coord. Chem. Rev.*, 2021, **446**, 214133.
10 J. K. Molloy, L. Fedele, O. Jarjayes, C. Philouze, D. Imbert and F. Thomas, *Inorg. Chim. Acta*, 2018, **483**, 609–617.
11 J. K. Molloy, O. Jarjayes, C. Philouze, L. Fedele, D. Imbert and F. Thomas, *Chem. Commun.*, 2017, **53**, 605–608.
12 R. Barré, D. Mouchel dit Leguerrier, L. Fedele, D. Imbert, J. K. Molloy and F. Thomas, *Chem. Commun.*, 2020, **56**, 435–438.
13 B. Wu, G. Warnock, M. Zaiss, C. Lin, M. Chen, Z. Zhou, L. Mu, D. Nanz, R. Tuura and G. Delso, *EJNMMI Phys.*, 2016, **3**, 19–19.
14 P. C. M. van Zijl and N. N. Yadav, *Magn. Reson. Med.*, 2011, **65**, 927–948.
15 G. Liu, X. Song, K. W. Y. Chan and M. T. McMahon, *NMR Biomed.*, 2013, **26**, 810–828.
16 K. J. Cai, H. N. Xu, A. Singh, L. Moon, M. Haris, R. Reddy and L. Z. Li, *Mol. Imaging Biol.*, 2014, **16**, 670–679.
17 F. Kogan, H. Hariharan and R. Reddy, *Curr. Radiol. Rep.*, 2013, **1**, 102–114.
18 D. Mouchel Dit Leguerrier, R. Barré, Q. Ruet, D. Imbert, C. Philouze, P. H. Fries, V. Martel-Frachet, J. K. Molloy and F. Thomas, *Dalton Trans.*, 2021, **50**, 10826–10837.
19 Q. N. Do, J. S. Ratnakar, Z. Kovács and A. D. Sherry, *ChemMedChem*, 2014, **9**, 1116–1129.
20 S. J. Ratnakar, T. C. Soesbe, L. L. Lumata, Q. N. Do, S. Viswanathan, C.-Y. Lin, A. D. Sherry and Z. Kovacs, *J. Am. Chem. Soc.*, 2013, **135**, 14904–14907.
21 F. Oukhatar, M. Beyler and R. Tripier, *Tetrahedron*, 2015, **71**, 3857–3862.
22 M. Milne, M. Lewis, N. McVicar, M. Suchy, R. Bartha and R. H. E. Hudson, *RSC Adv.*, 2014, **4**, 1666–1674.
23 L. Ma, C. Xie, Y. Ma, J. Liu, M. Xiang, X. Ye, H. Zheng, Z. Chen, Q. Xu, T. Chen, J. Chen, J. Yang, N. Qiu, G. Wang, X. Liang, A. Peng, S. Yang, Y. Wei and L. Chen, *J. Med. Chem.*, 2011, **54**, 2060–2068.
24 R. Pujales-Paradela, T. Savić, P. Pérez-Lourido, D. Esteban-Gómez, G. Angelovski, M. Botta and C. Platas-Iglesias, *Inorg. Chem.*, 2019, **58**, 7571–7583.

25 R. Pujales-Paradela, T. Savić, D. Esteban-Gómez, G. Angelovski, F. Carniato, M. Botta and C. Platas-Iglesias, *Chem. – Eur. J.*, 2019, **25**, 4782–4792.
26 K. Binnemans, *Chem. Rev.*, 2009, **109**, 4283–4374.
27 R. M. Supkowski and W. D. Horrocks, *Inorg. Chim. Acta*, 2002, **340**, 44–48.
28 A. Beeby, I. M. Clarkson, R. S. Dickins, S. Faulkner, D. Parker, L. Royle, A. S. de Sousa, J. A. Gareth Williams and M. Woods, *J. Chem. Soc., Perkin Trans. 2*, 1999, 493–504, DOI: 10.1039/A808692C.
29 G. Ionita, V. Meltzer, E. Pincu and V. Chechik, *Org. Biomol. Chem.*, 2007, **5**, 1910–1914.
30 L. A. Basal, M. D. Bailey, J. Romero, M. M. Ali, L. Kurenbekova, J. Yustein, R. G. Pautler and M. J. Allen, *Chem. Sci.*, 2017, **8**, 8345–8350.
31 T. Gambino, L. Valencia, P. Pérez-Lourido, D. Esteban-Gómez, M. Zaiss, C. Platas-Iglesias and G. Angelovski, *Inorg. Chem. Front.*, 2020, **7**, 2274–2286.
32 E. Vinogradov, A. D. Sherry and R. E. Lenkinski, *J. Magn. Reson.*, 2013, **229**, 155–172.
33 S. J. Ratnakar, S. Viswanathan, Z. Kovacs, A. K. Jindal, K. N. Green and A. D. Sherry, *J. Am. Chem. Soc.*, 2012, **134**, 5798–5800.
34 R. Wu, G. Xiao, I. Y. Zhou, C. Ran and P. Z. Sun, *NMR Biomed.*, 2015, **28**, 376–383.
35 S. A. A. S. Subasinghe, J. Romero, C. L. Ward, M. D. Bailey, D. R. Zehner, P. J. Mehta, F. Carniato, M. Botta, J. T. Yustein, R. G. Pautler and M. J. Allen, *Chem. Commun.*, 2021, **57**, 1770.
36 A. C. L. Opina, Y. Wu, P. Zhao, G. Kiefer and A. D. Sherry, *Contrast Media Mol. Imaging*, 2011, **6**, 459–464.
37 R. Barré, D. Mouchel dit Leguerrier, Q. Ruet, L. Fedele, D. Imbert, V. Martel-Frachet, P. H. Fries, J. K. Molloy and F. Thomas, *Chem. – Asian J.*, 2022, e202200544.
38 D. Kovacs, E. Matthieu, S. R. Kiraev, J. A. L. Wells, E. Demeyere, A. SIpos and K. E. Borbas, *J. Am. Chem. Soc.*, 2020, **142**(30), 13190–13200.